Common and atypical PET/CT features of non-malignant musculoskeletal processes

R. S. Plowman, M.D.; B. D. Nguyen, M.D.

Department of Radiology, Mayo Clinic, Scottsdale, AZ, USA

Corresponding author: nguyen.ba@mayo.edu

Category: Education Review 080 (ER_080)

OBJECTIVES

- (1) to present the F-18 FDG PET/CT musculoskeletal features related to physiologic variants, medically-induced processes, inflammation, infection, injury, iatrogenic and post-operatives changes, and benign soft tissue and osseous lesions, and

- (2) to discuss the patterns of recognition of PET/CT features and, whenever necessary, the correlation with other imaging modalities in order to differentiate benign musculoskeletal processes from malignant lesions.

Authors' disclosure: no conflict of interest to declare.

PICTORIAL ESSAY

The exhibit encompasses musculoskeletal PET/CT features, depicted incidentally or purportedly during oncologic functional imaging, representing:

- Volunteer and unintended muscle contractions such as jaw clenching, seizure, and breathing effort in emphysema,
- Brown adipose soft tissue,
- Post-radiation and post-chemotherapy impact on bone marrow, tendinous insertion, bursa and joint spaces,
- Trauma and insufficiency/stress injury,
- Drug-induced and iatrogenic causes such as insulin administration, anticoagulant-related hematoma, sternotomy, ischiocavernosus myositis, and sequela of cardiopulmonary resuscitation,
- Benign entities such as odontogenic cyst, enchondroma, bone infarction, hemangioma, island of red bone marrow, aneurysmal bone cyst, pigmented villonodular synovitis, ischiogluteal bursitis, arthroplasty-related foreign body granulomatous formation, osteomyelitis, myositis ossificans, elastofibroma dorsi, desmoid tumor, hemorrhagic pseudotumor, schwannoma, solitary fibrous tumor, sarcoidosis and phosphaturic mesenchymal tumors inducing oncogenic osteomalacia.

Masseteric muscles clenching

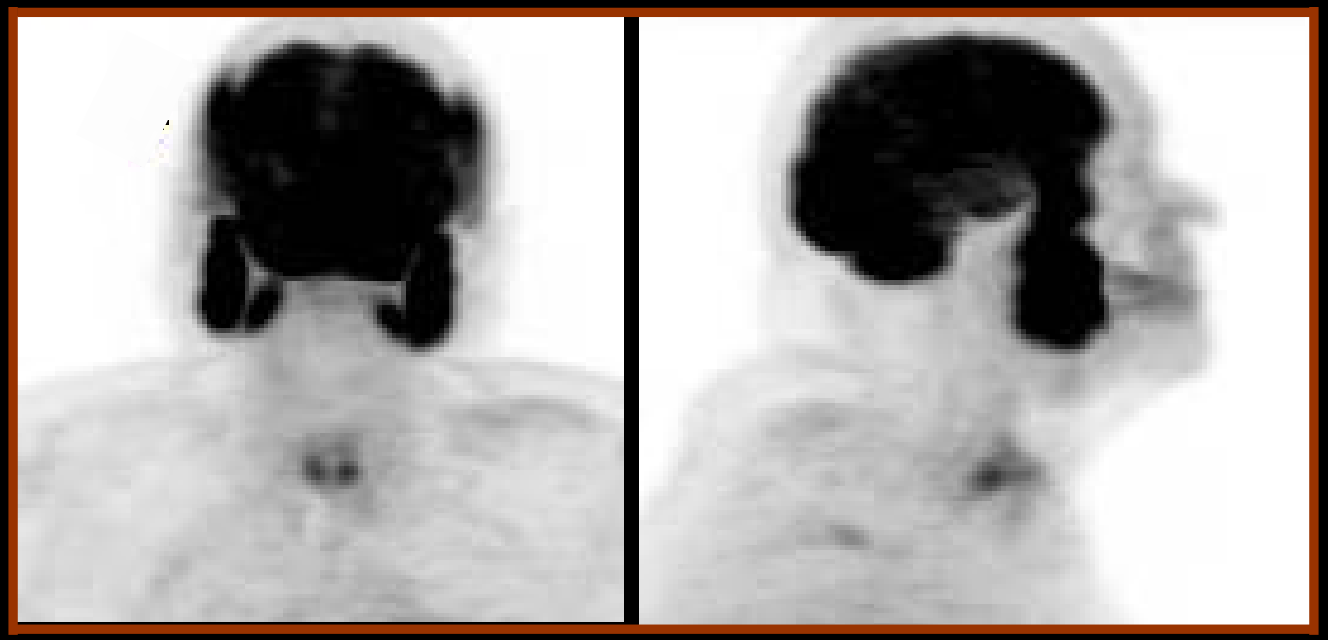

PET MIP (left) and fused PET/CT (above) images demonstrate the hypermetabolic soft tissue features of the muscles of mastication during the acquisition phase of positron emission tomography.

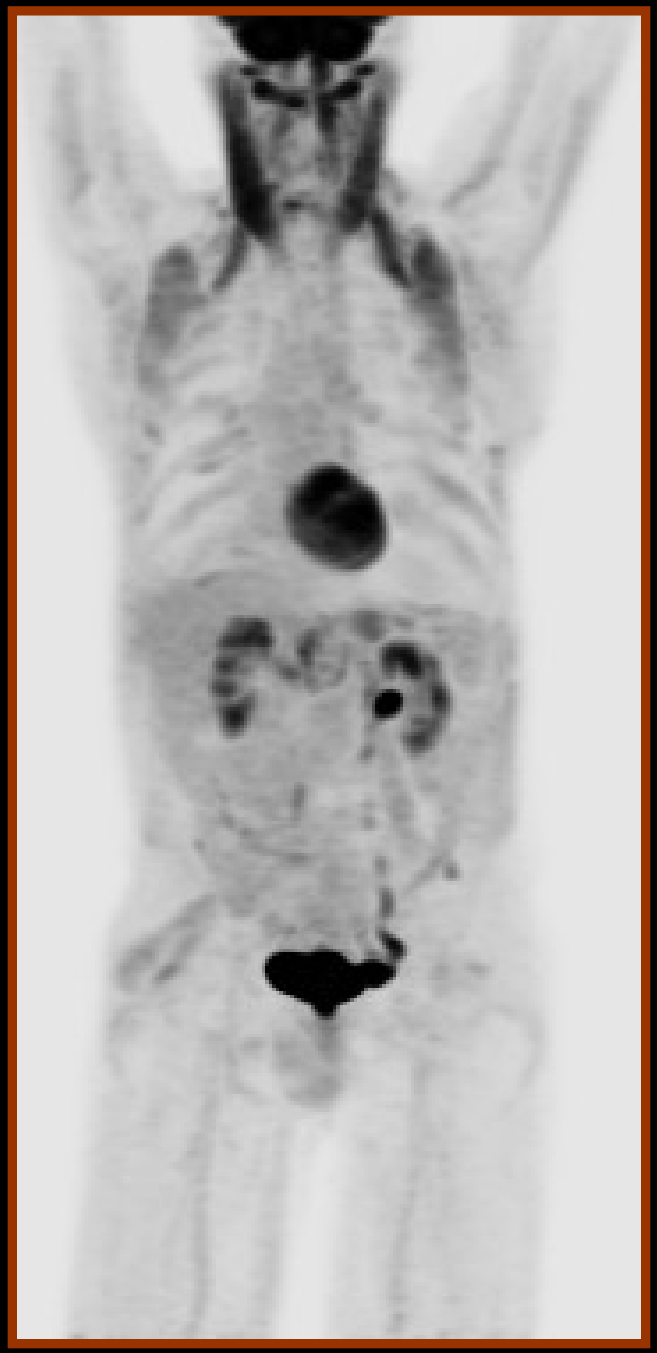

Muscle contractions in emphysema

PET MIP image demonstrates the hypermetabolic soft tissue features of the muscles in use owing to the increased work of breathing from emphysema during the image acquisition

Involuntary muscle contraction

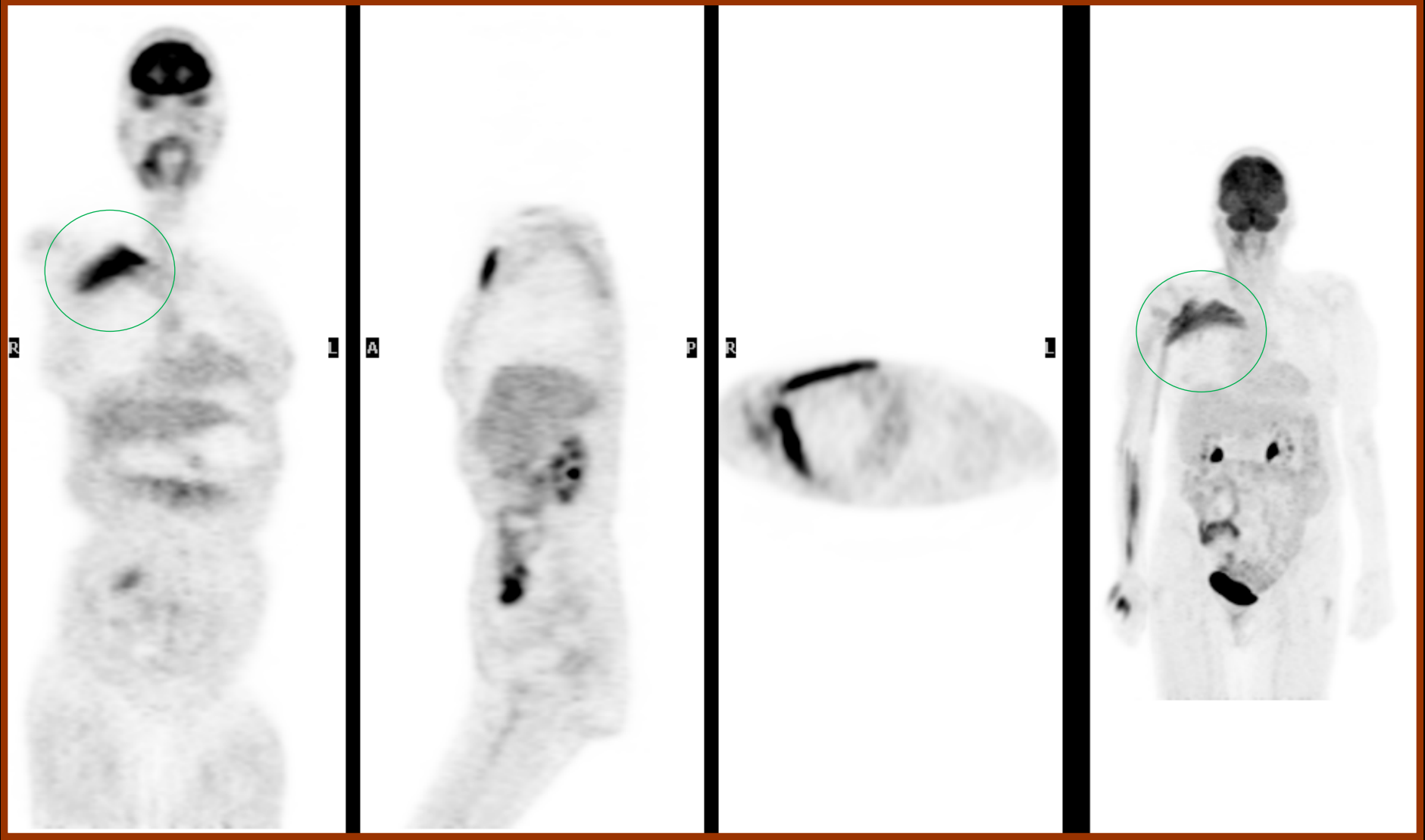

Whole body PET coronal, sagittal, axial and volumetric images showed abnormal radiotracer uptake at the musculature of the right neck, right shoulder girdle predominantly at the pectoralis major and subscapularis muscles (circled), and entire right upper extremity due to involuntary dyskinetic muscular exertion of recent seizure.

Elastofibroma dorsi

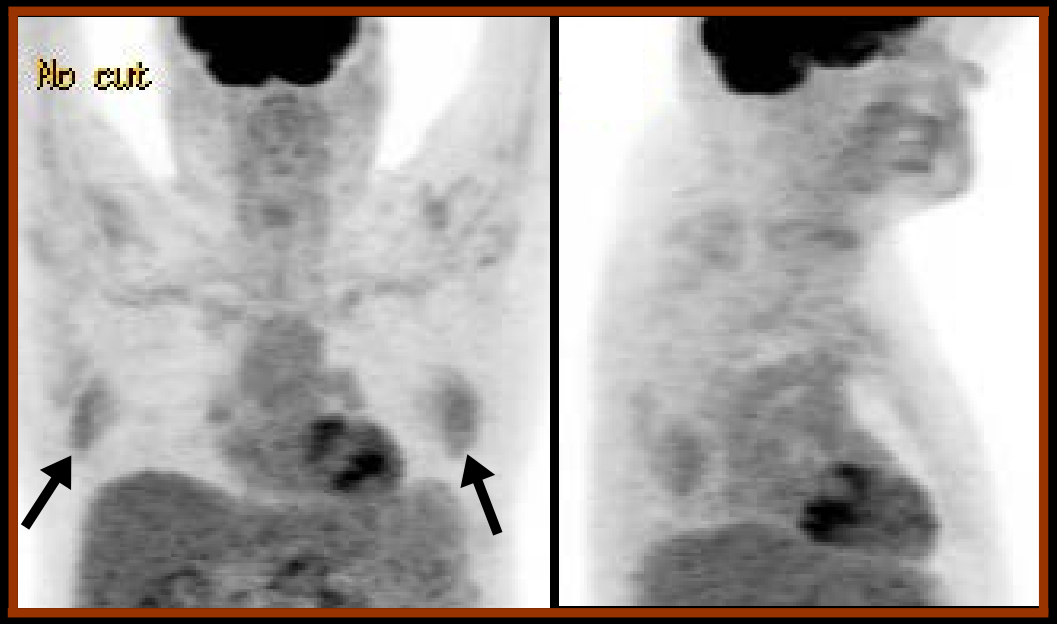

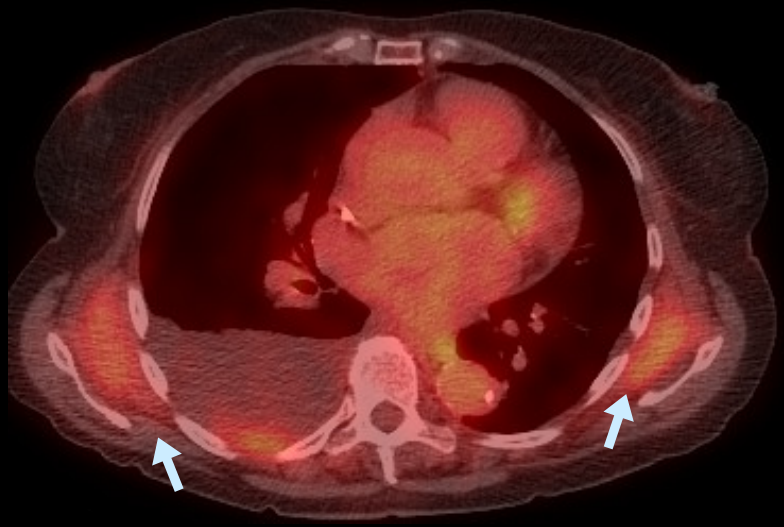

PET MIP and PET/CT images showing hypermetabolic soft tissue features of the chest wall bilaterally located between the rib cage and the inferior aspect of both scapulae exhibiting mild to moderately intense patchy pattern of tracer uptake. The PET features with corresponding CT soft tissue/fat attenuation characteristics are suggestive of elastofibroma dorsi (arrows)

Desmoid tumor

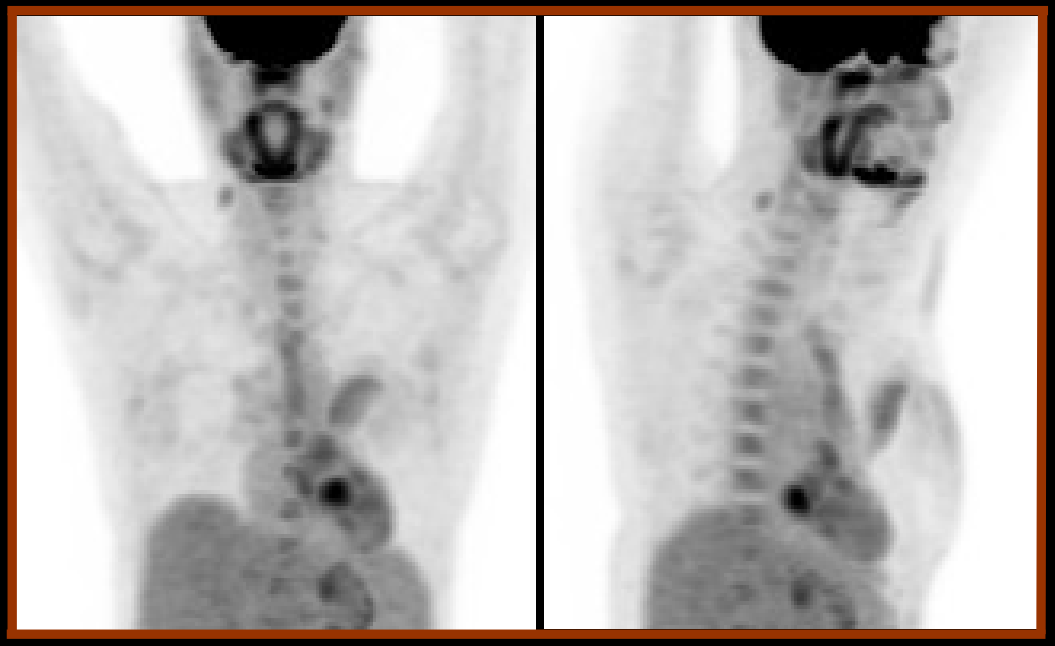

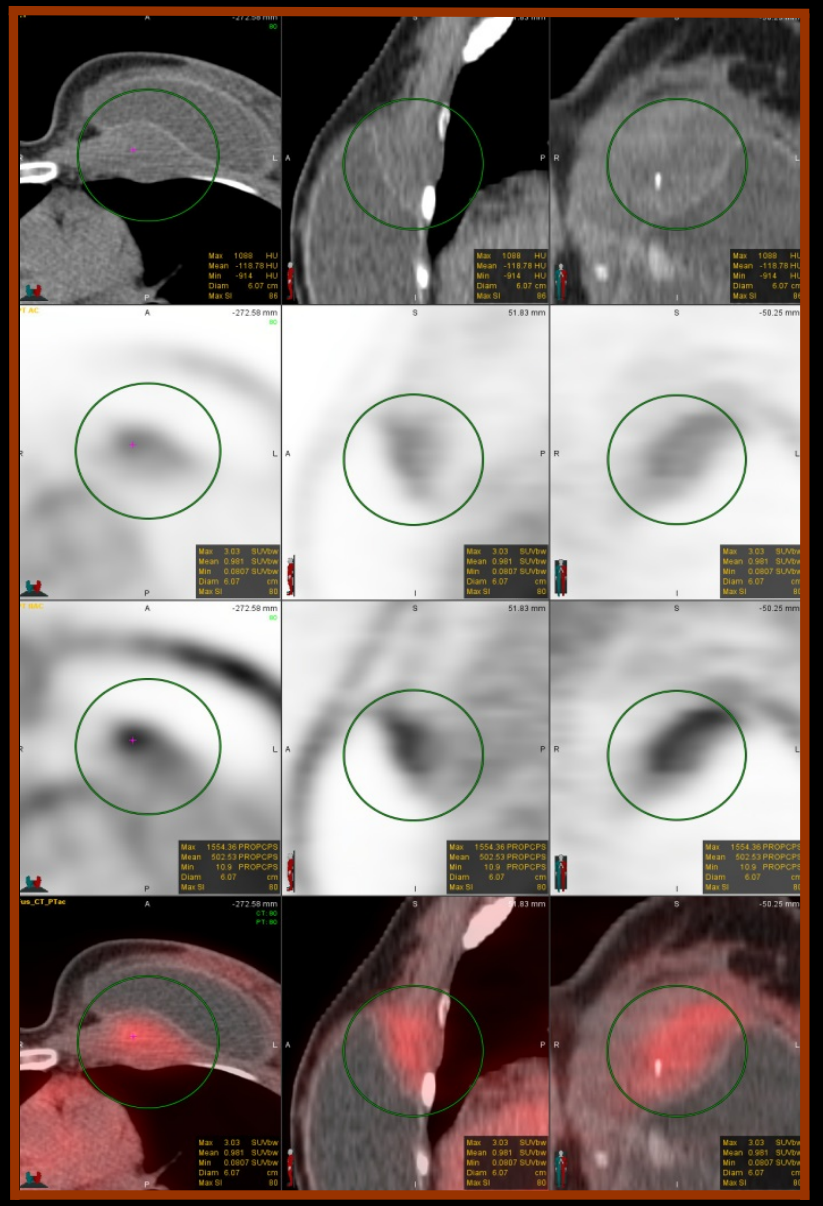

PET MIP and PET/CT images showing hypermetabolic soft tissue features of the left chest wall located between the rib cage and the breast implant. This exhibits a mild/moderate intensity pattern of tracer uptake. The PET features with corresponding CT soft tissue/fat attenuation characteristics are suggestive of desmoid tumor (green circles).

Sequella of TRAM flap surgery

PET MIP images showing the sequelae of transverse rectus abdominal muscle (TRAM) flap surgery as a method of breast reconstruction, by using a flap of abdominal tissue with corresponding hypermetabolic soft tissue features along the anterior abdominal wall resulting from granulomatous inflammation (arrows).

Insulin injection

PET MIP images showing the undesirable diffuse muscle uptake features from insulin injection prior to undergoing positron emission tomography acquisition utilizing F-18 FDG. Insulin facilitates the incorporation of F-18 FDG in muscles interfering with the detection of any tracer-avid malignant lesion.

Non-fasting

PET MIP images showing the diffuse muscle uptake features of a patient who was not compliant with the pre-exam instructions of fasting at least 6 hours prior to undergoing positron emission tomography acquisition utilizing F-18 FDG. Sugar consumption just prior to PET imaging results in similar PET features seen in patients with recent insulin administration.

Brown adipose tissue

Whole body PET MIP image showed the classic bilateral and symmetrical pattern of hypermetabolic brown adipose tissue (BAT) at the sub-occipital, cervical, supraclavicular, axillary, and paraspinal regions (left figure). Composite PET/CT images showed a mid-line upper thoracic single focus of F-18 FDG uptake (SUV: 8) corresponding to the BAT at the supra-sternal notch on transmission CT (right figure).

Bilateral rib fractures from CPR

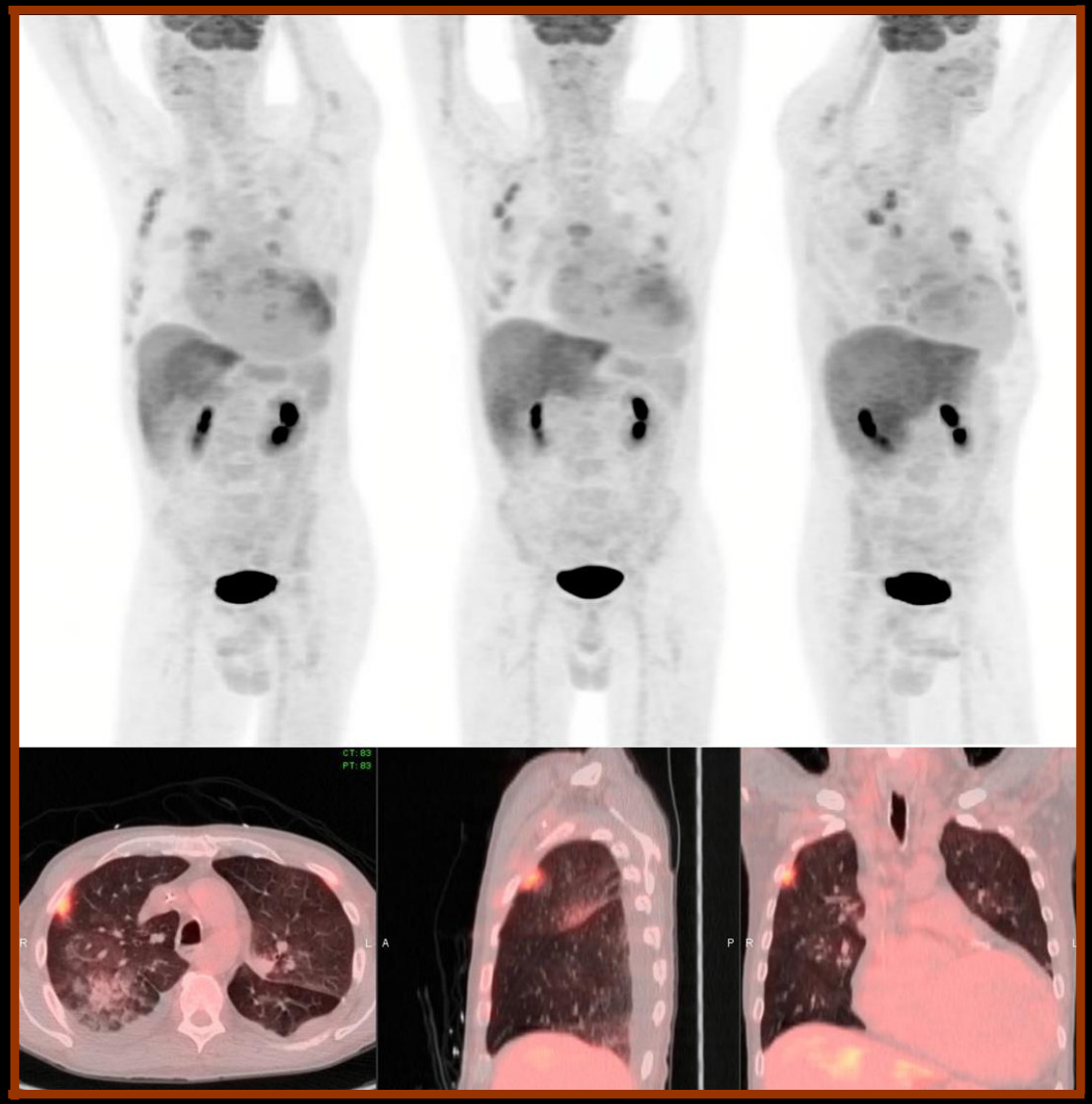

PET MIP and fused PET/CT images showing the bilaterally aligned rib fractures from recent CPR with associated lung contusion in a patient with cardiac amyloidosis.

Fracture of sternum

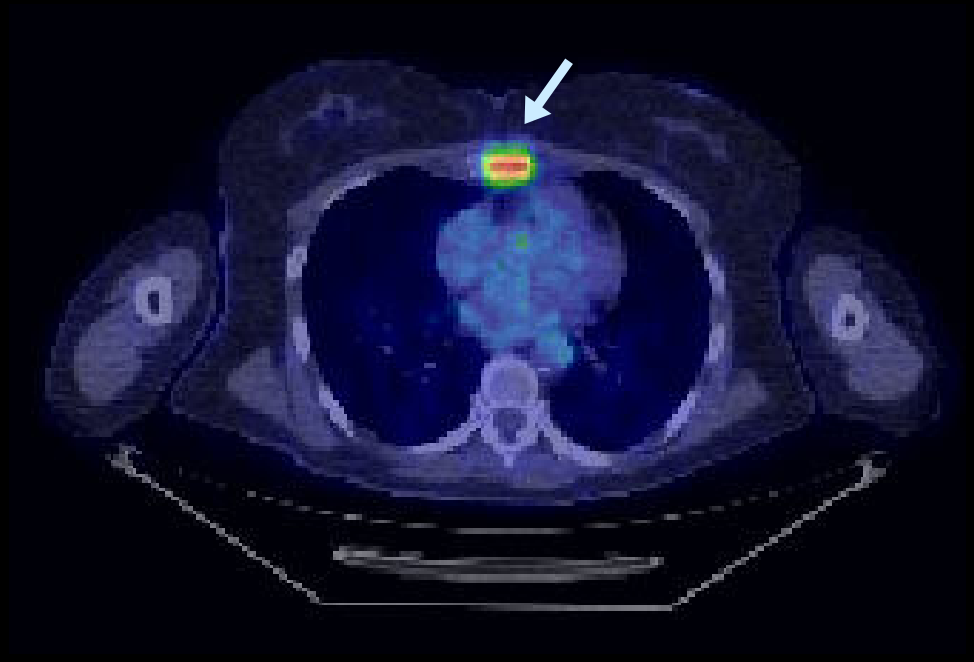

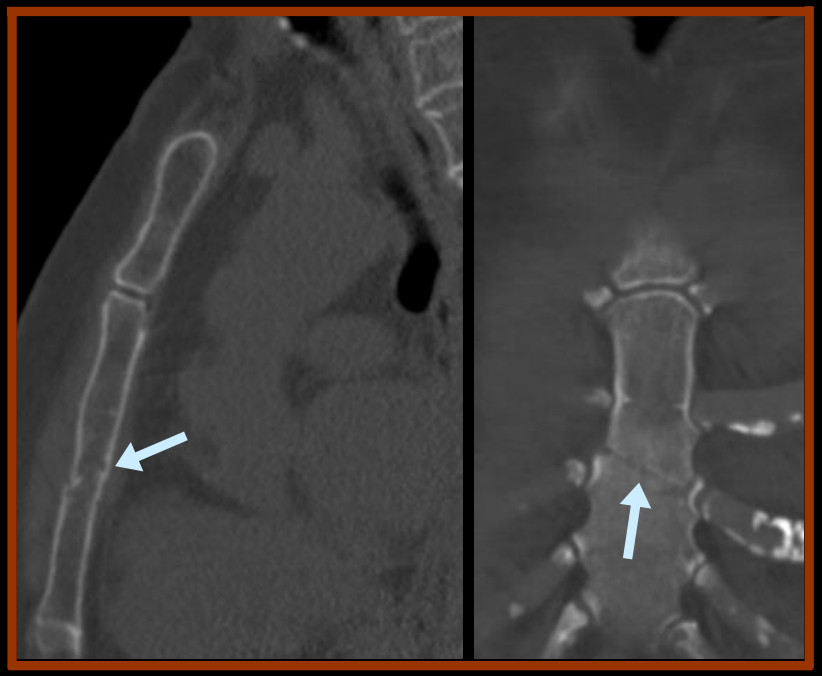

Axial PET image (left) shows increased tracer uptake from a healing sternal fracture (arrow). CT reconstruction images in the sagittal and coronal projections (middle & right) show subtle fracture-deformity of the sternum overlooked on initial interpretation (arrows).

Sternotomy

Tracer uptake on fused PET/CT images (arrows) from post-operative changes of the sternotomy. The diffuse features of uptake of the sternum along with sternal wiring usually represent a benign process rather than malignancy.

Reactive bone marrow

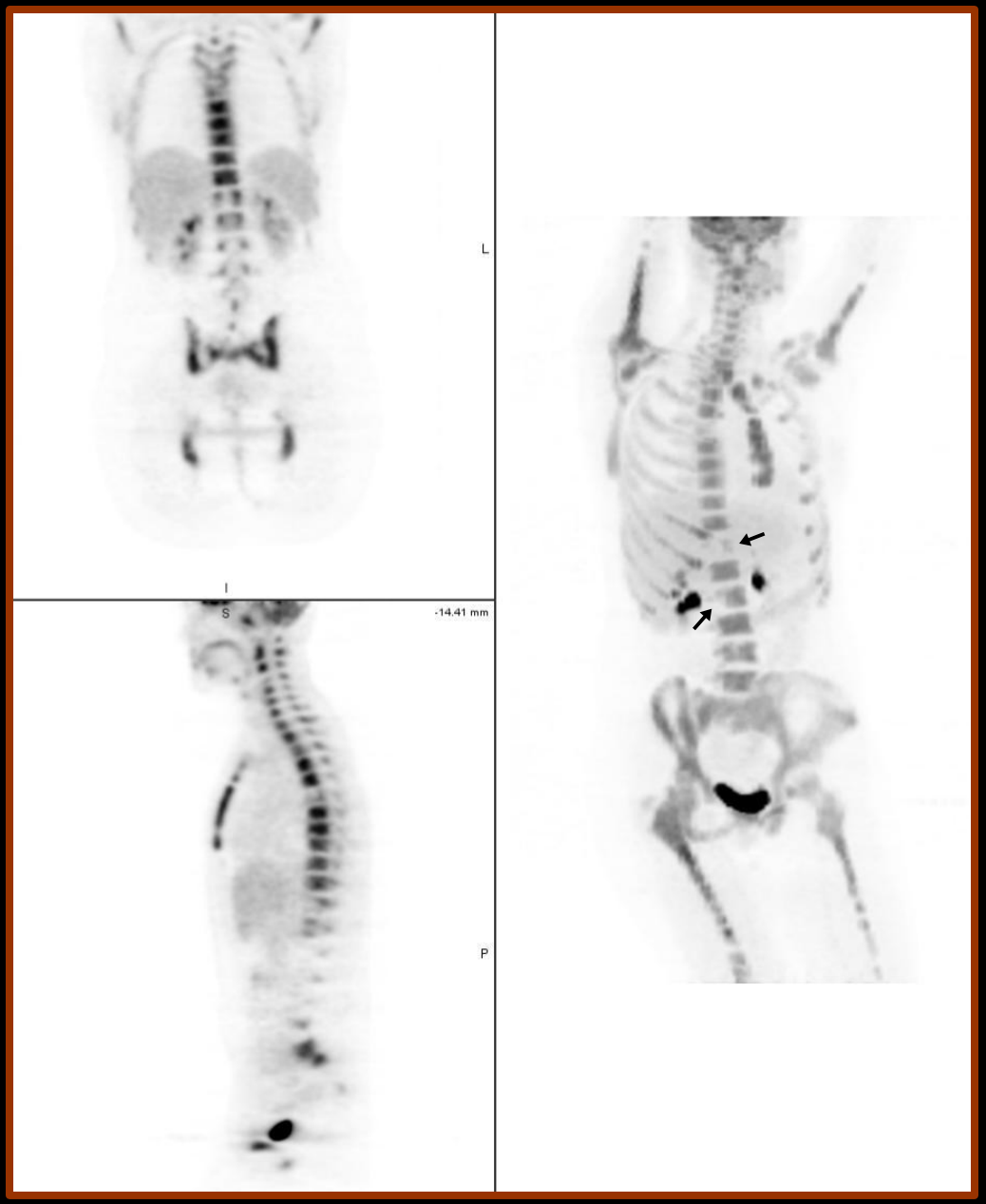

Reactive bone marrow from post-therapeutic changes. The PET images show two different patients with diffuse axial and appendicular skeletal uptake after chemotherapy. A few foci of osseous tracer defect in the right are related to sclerotic bone marrow from treated metastases (arrows).

Schwannomas

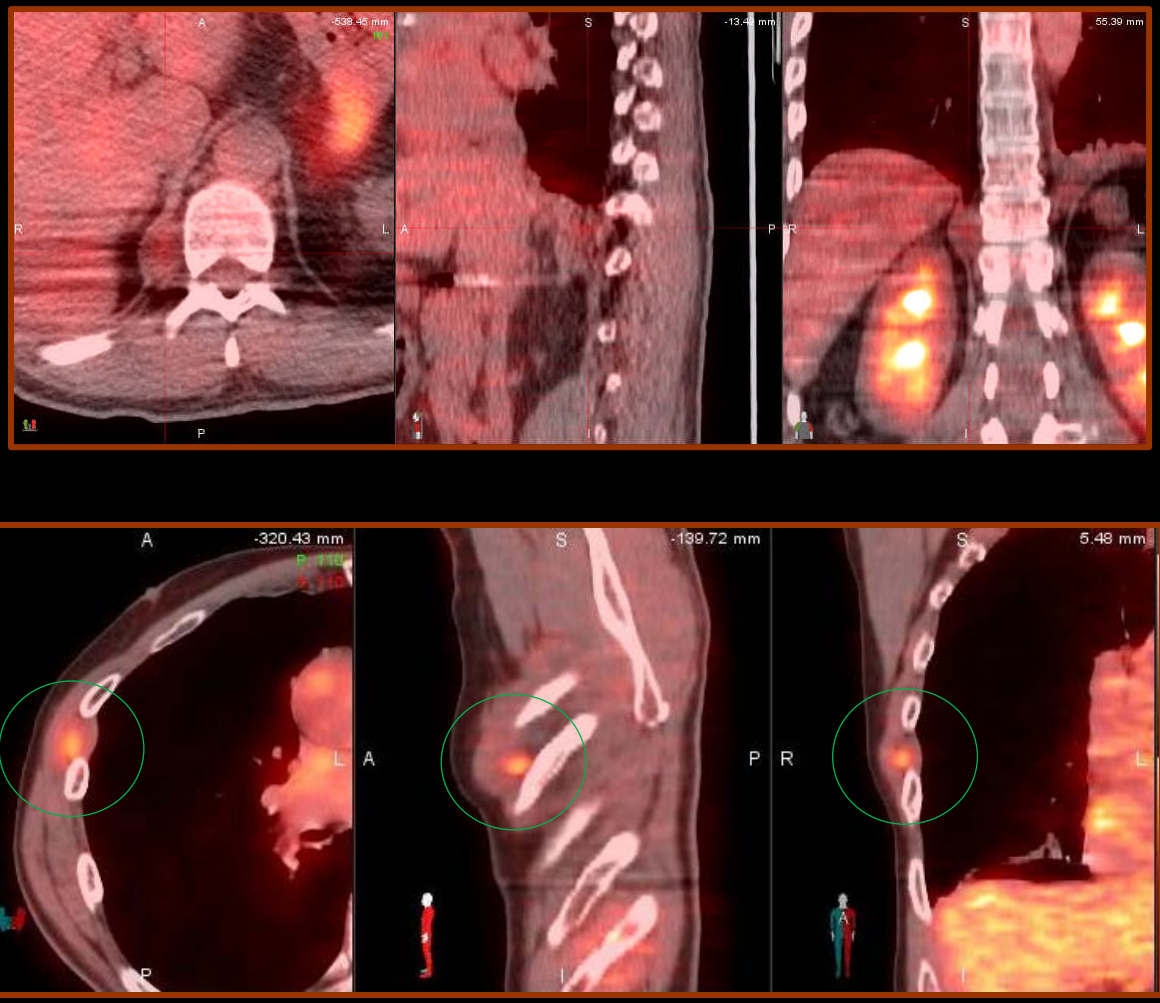

Different levels of hypermetabolic behavior of schwannoma at the right retrocrural region (top row) and at right intercostal space (bottom row) mimicking nodal or soft tissue malignant lesions (green circles).

Schwannomas, cont.

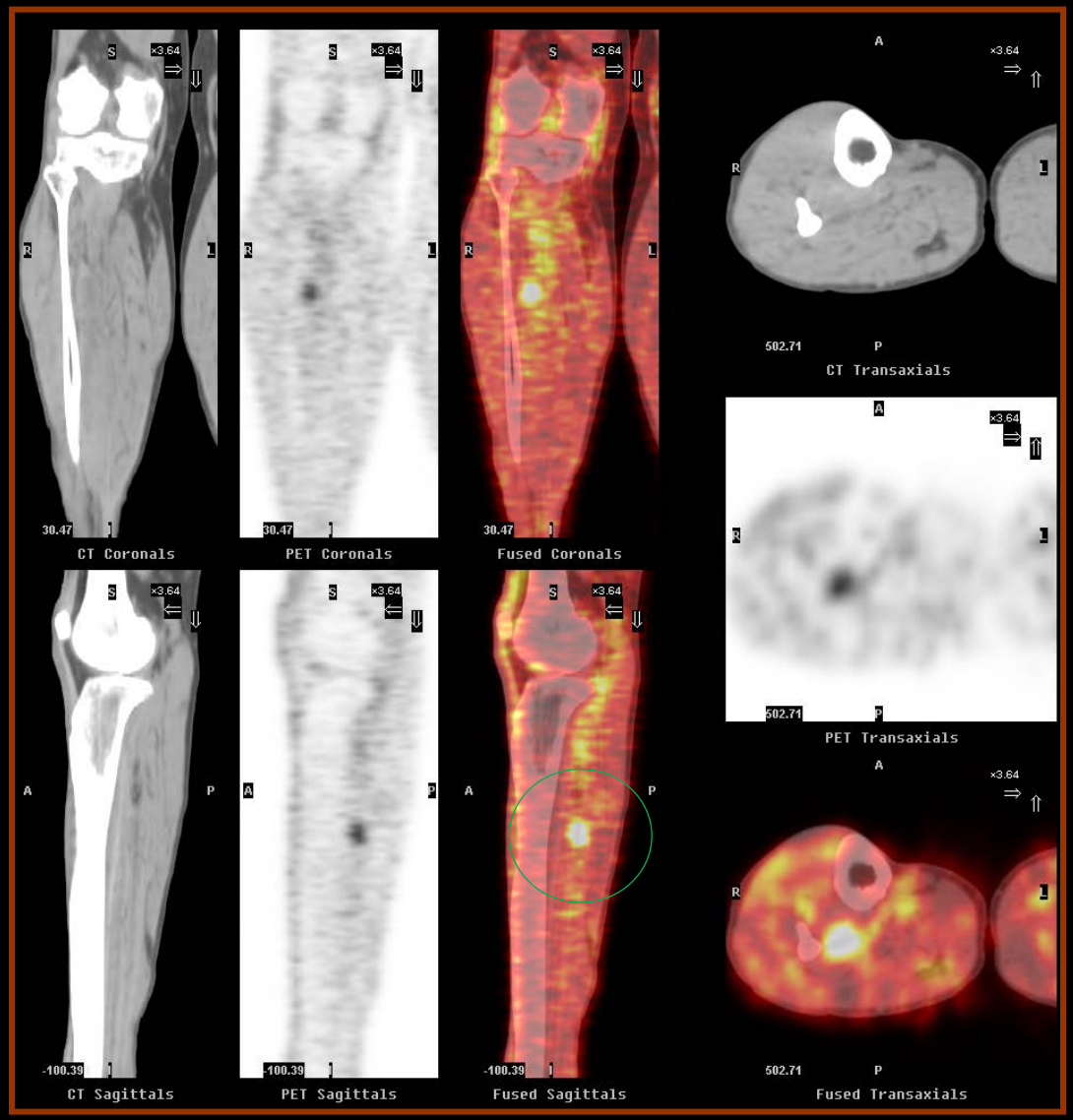

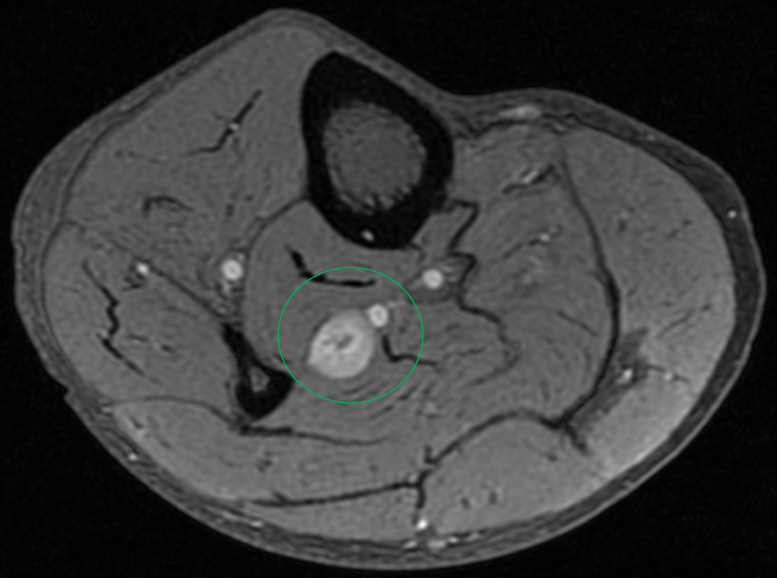

Patient with history of treated metastatic malignant melanoma. Restaging PET/CT imaging shows an abnormal radiotracer uptake in the right calf (left figure) matching the enhancing lesion on subsequent MR examination (circled) of the right lower extremity (right figure). The patient underwent surgery for suspected calf metastasis from melanoma. The final diagnosis is a schwannoma.

Red bone marrow island

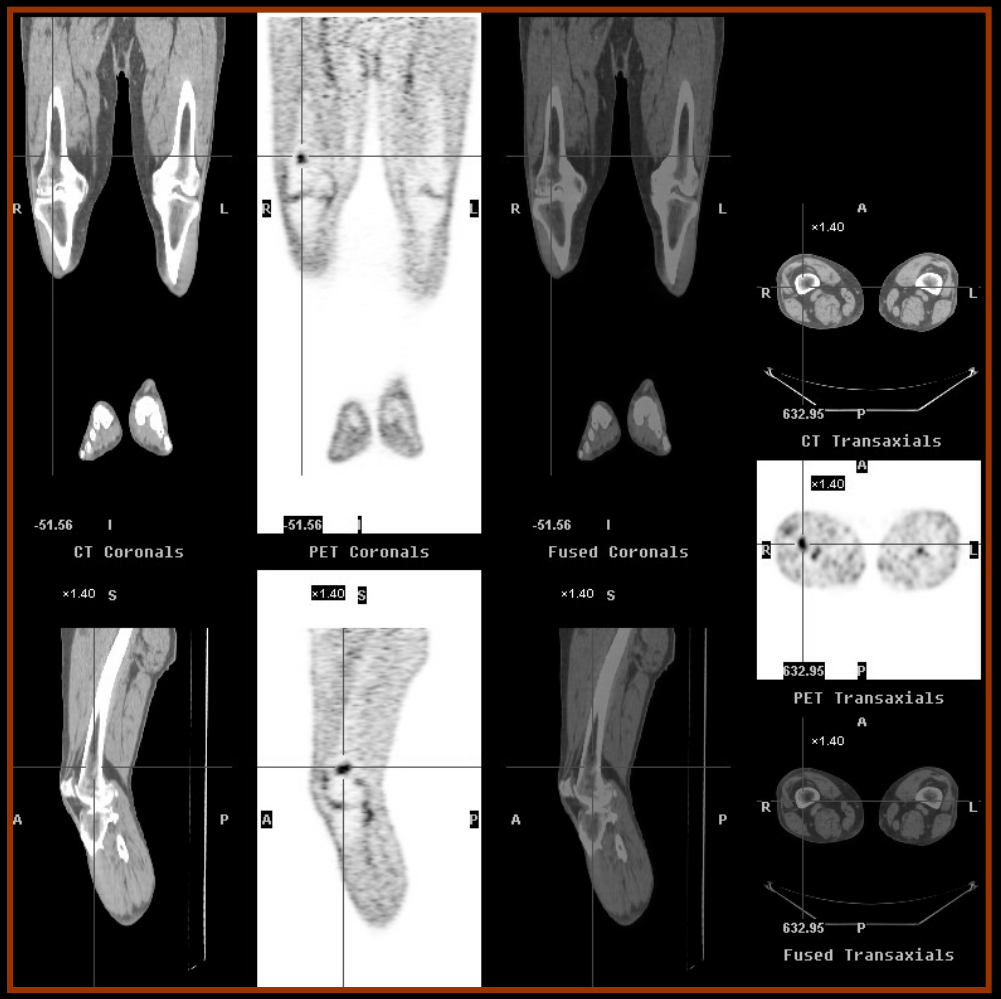

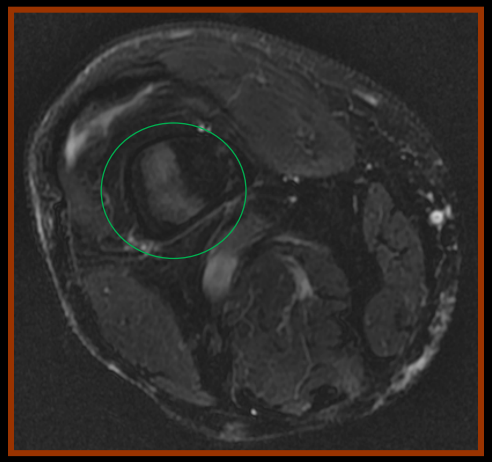

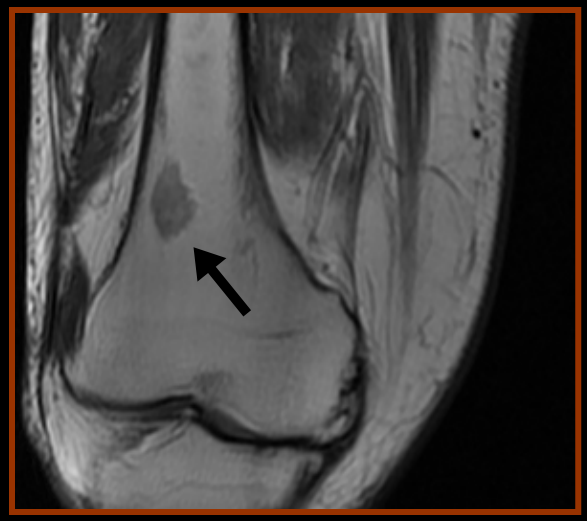

PET/CT shows a focus of increased radiotracer accumulation at the distal right femur (left figure, crosshair, SUV: 3.7) corresponding to subtle focal bone marrow increased attenuation on co-registered CT. MR shows a well-demarcated focus of mildly decreased signal intensity (black arrow) on T1-weighted coronal image (bottom right) and mildly increased signal intensity (green circle) on T2-weighted axial image (top right) comparing to adjacent bone marrow of the distal right femur. This focus also exhibited a drop in signal intensity on opposed-phase MR imaging sequences (not shown) suggesting the presence of fat tissue component. All these MR features were consistent with an island of benign red marrow.

Vertebral hemangioma

Coronal PET images show focal tracer defect at the left aspect of L2 vertebra (arrow) corresponding to the hemangioma depicted by the axial CT (left figure) and MR (right figure) images (circles)

Aneurysmal bone cyst

PET/CT showed increased uptake in the lobulated lesion at T9 with SUV of 8.7 (left figure). MRI of thoracic spine showing the right T9 pedicle lesion with combined solid/enhancing and non-enhancing cystic components (upper right figure). The mass also involves the vertebral body, transverse process, and lamina as circled in the corresponding CT axial image (lower right figure).

Insufficiency fractures

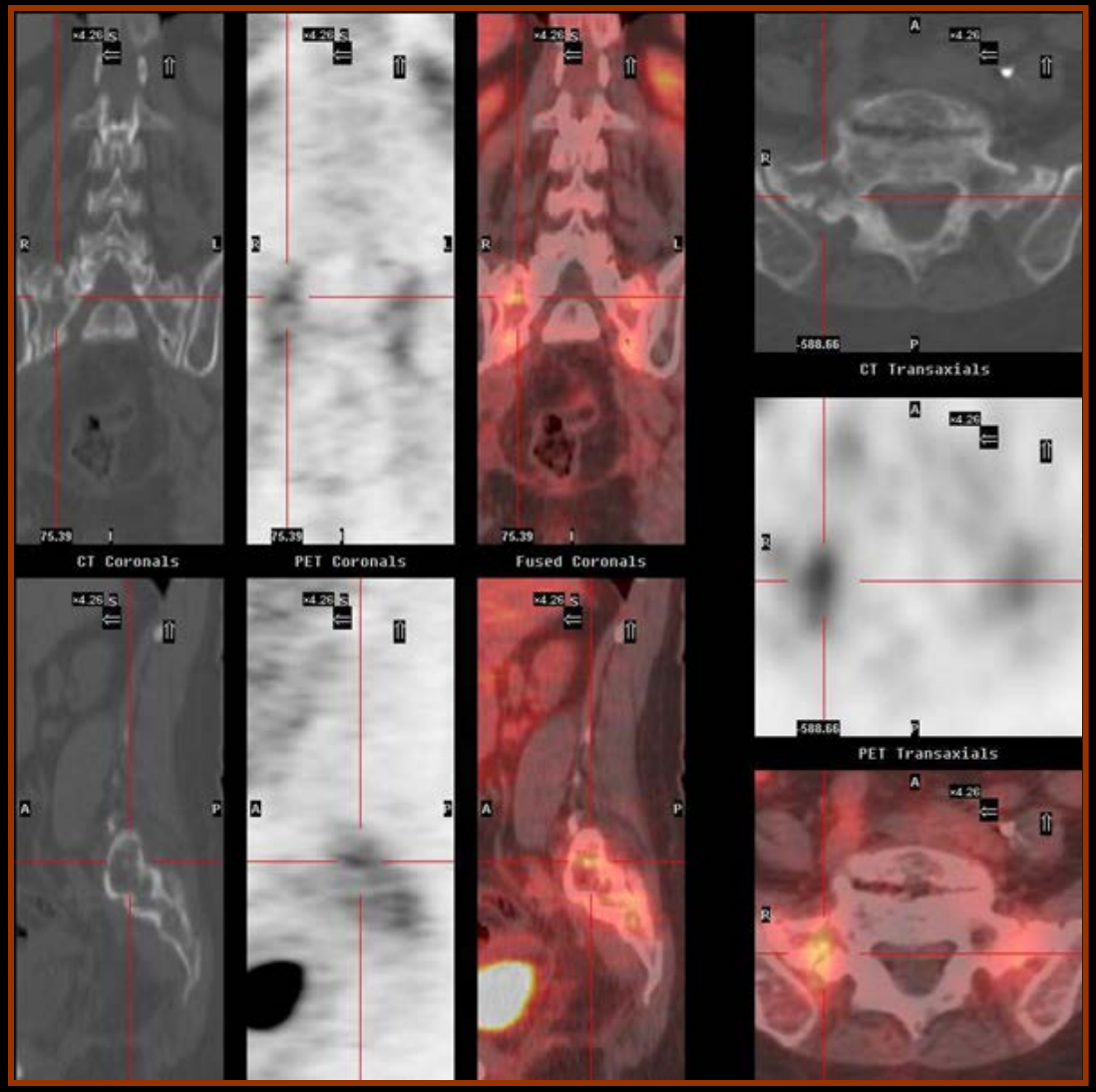

PET/CT shows bilateral curvilinear tracer uptake at the sacral alae from CT-depicted sacral insufficiency fractures

Soft tissue injury

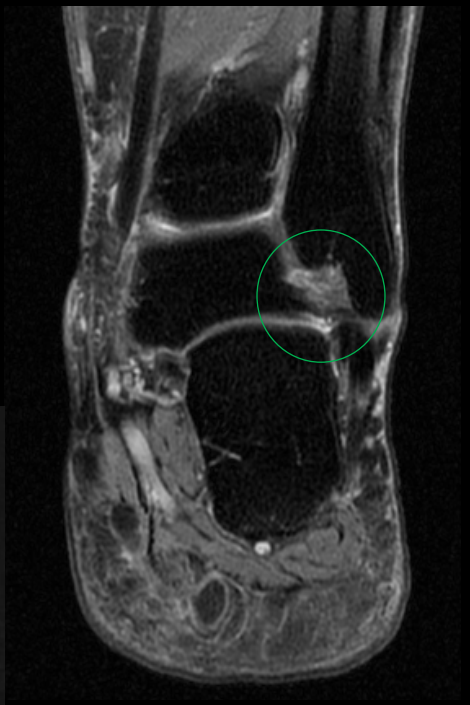

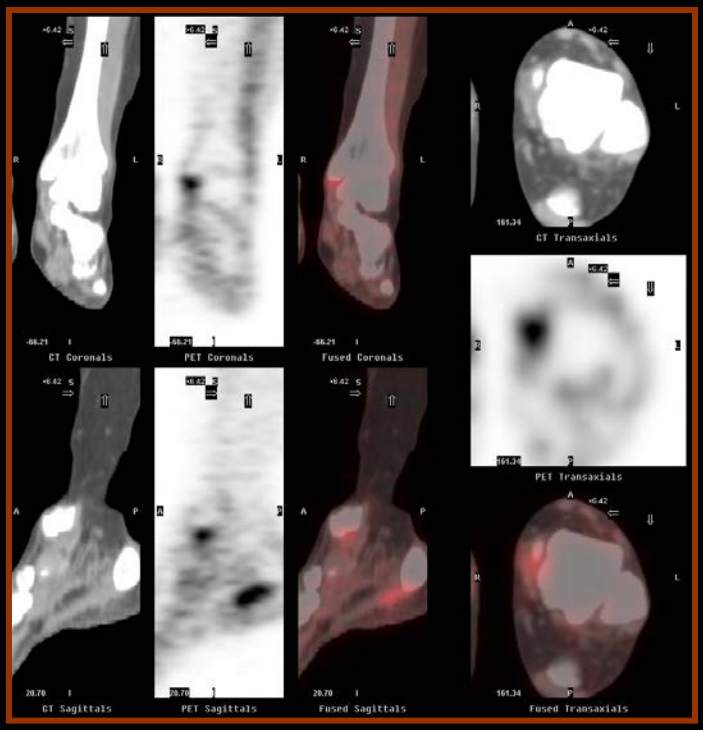

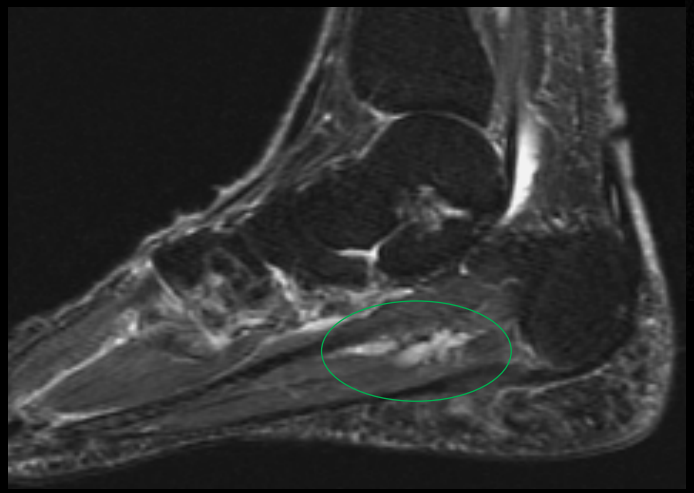

PET/CT (top left and right images) show abnormal tracer accumulation at the medial aspect of the left ankle (SUV: 2.5) and at the plantar aspect of the left foot (SUV 2.8) respectively. Coronal MR image (middle figure) shows a partial tear of the tibiocalcaneal ligament just distal to the left medial malleolus matching the PET finding. Sagittal MR image (bottom left) shows a subacute partial tear at the posteromedial aspect of the left plantar fascia corresponding to the PET finding.

Ischiogluteal bursitis

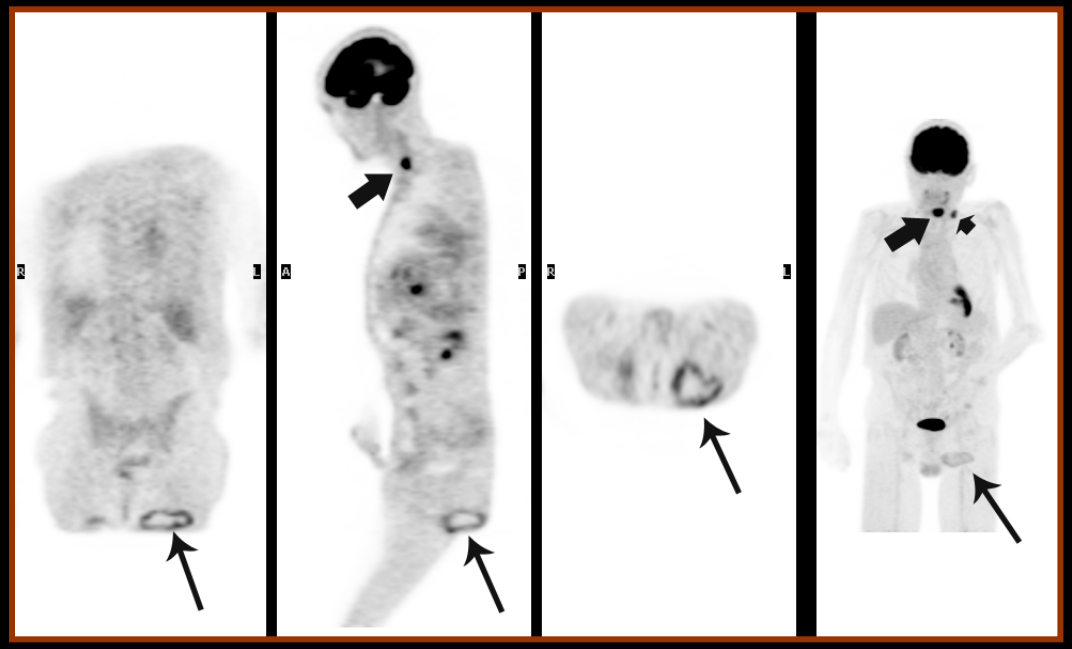

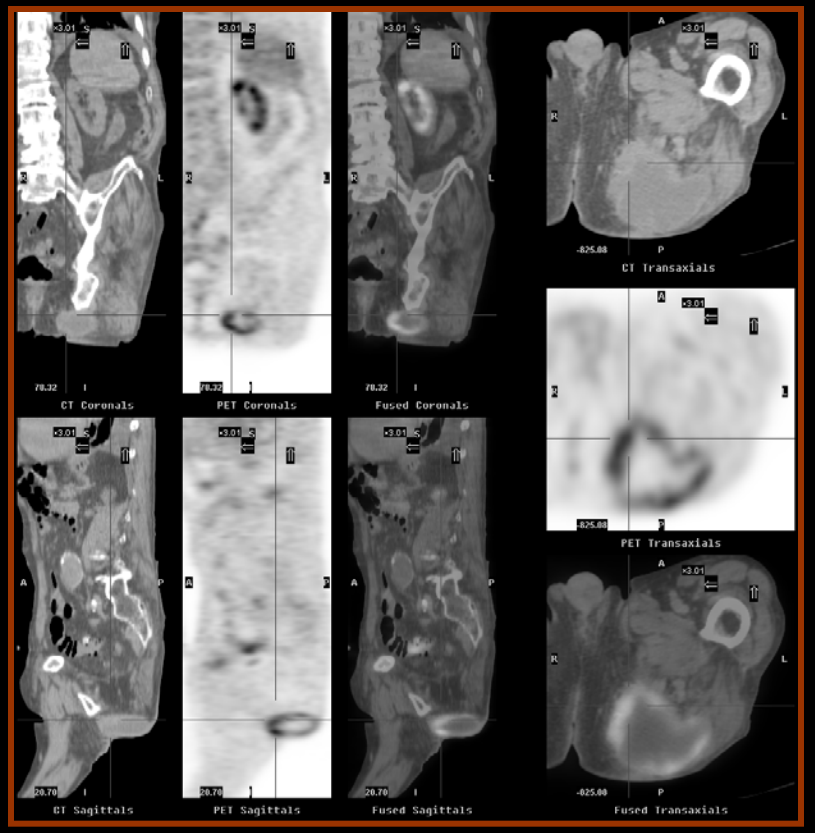

Coronal, sagittal, axial and MIP PET images (left figure) show a ring-like focus of abnormal radiotracer accumulation at the inferior aspect of the left pelvis (long arrows) in a patient with neck malignancy (shorter arrows). Composite PET/CT image (right figure) of the left lower pelvis showed a peripherally hypermetabolic lesion corresponding to an 8-cm cystic mass located between the left ischium and gluteus muscles (crosshair, SUV: 3). The patient had a history of rheumatoid arthritis with known prior ischiogluteal bursitis (IGB). The present cystic lesion, non-tender on palpation, probably represented a large recurrent IGB.

THA foreign body reaction

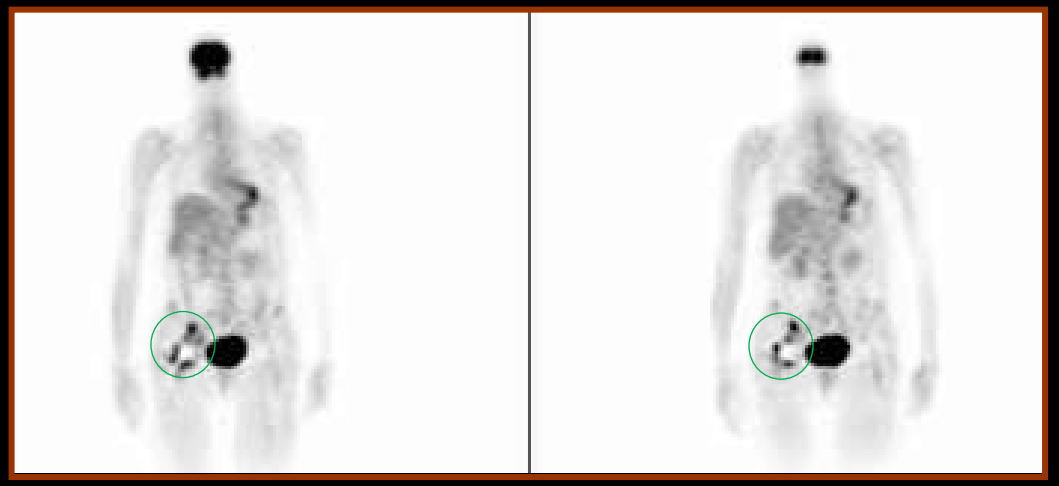

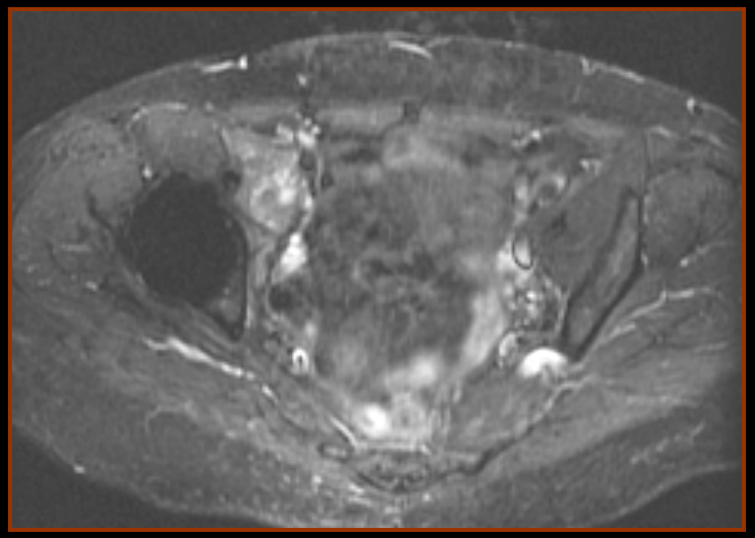

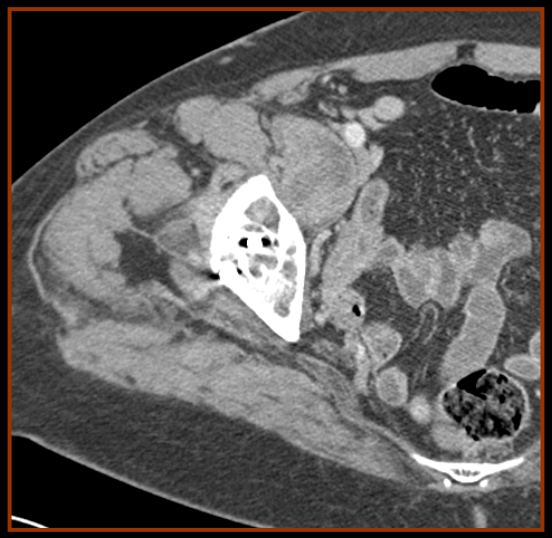

A patient with a 8-year-old right total hip arthroplasty (THA) consisting of a Zimmer Centralign Precoat femoral prosthesis and a polyethylene Osteonics peripherally-self-locking acetabular component. She had an onset of right hip spasm and pain with palpable right pelvic-inguinal mass suspicious for recurrent melanoma. MR shows a complex lesion involving the right ilio-psoas bursa (bottom left). PET images (top right) show a lobulated focus of abnormal tracer accumulation (circle) at the right supra-acetabular region medially matching the MR finding. Pelvic CT axial (bottom middle) and coronal (bottom right) images confirm the soft tissue lesion. Tissue sampling shows histologic evidence of granulomatous disease with no infection or malignancy. Surgery finds an aseptic loosening THA.

Sarcoidosis

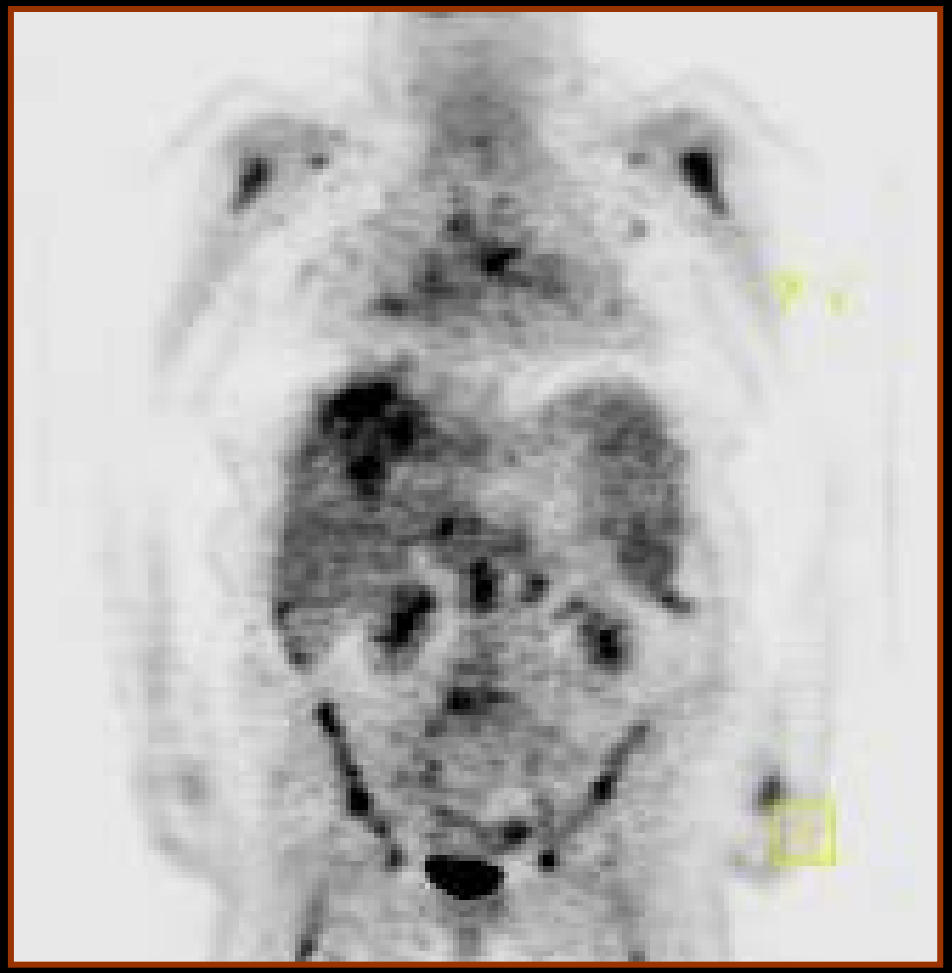

Coronal whole body F-18 FDG PET images show disseminated foci of radiotracer uptake liver, axial and appendicular skeleton, and mediastinal and hilar nodes. The diffuse hepatic high metabolic lesions appear patchy, confluent and mass-like predominantly in the left hepatic lobe. These diffuse hypermetabolic features of sarcoidosis mimic advanced metastasis.

Pigmented villonodular synovitis

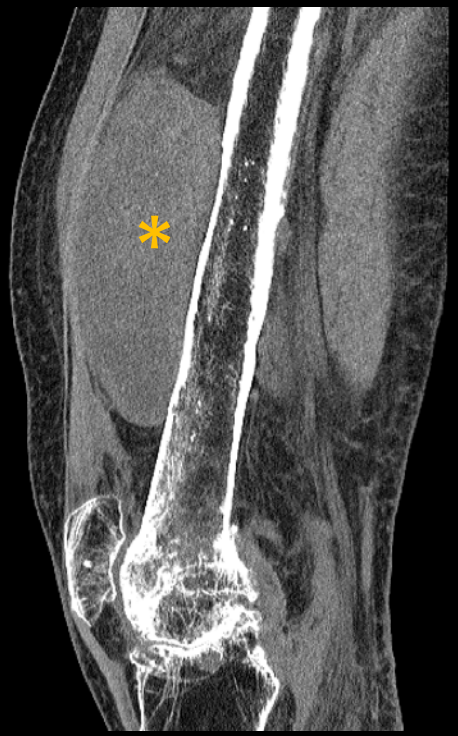

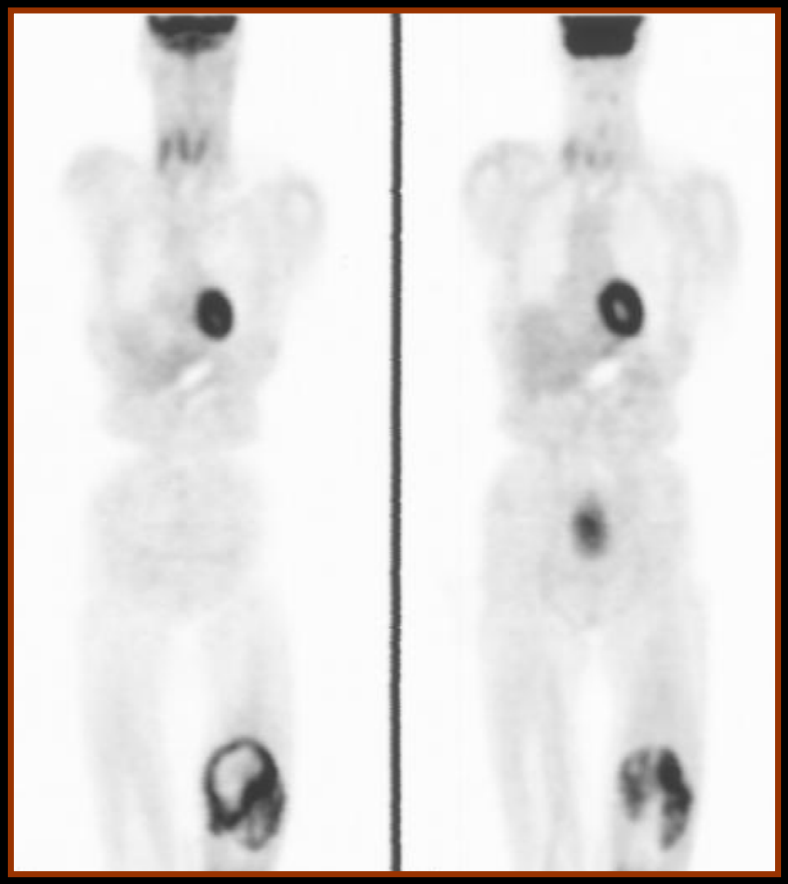

MR coronal image (left figure) shows an enlarging lobulated 10 x 7 x 13 cm left thigh mass compressing or invading the vastus intermedialis muscle. This heterogeneously contrast enhancing lesion is abutting or in communication with the suprapatellar bursa. CT sagittal image (middle figure) showed the non-calcified thigh mass (asterisk) with pressure erosion on the anterior distal femoral cortex and marked degenerative disease of the left knee join. PET coronal images (right figure) show a large soft tissue focus of abnormal radiotracer accumulation partially wrapping around the mid and distal aspects of the left femur. There were photon-deficient geographic areas within the large mass probably related to loculated fluid collection or tissue necrosis matching MR features. Due to the aggressive MR features and positive PET findings, a repeat biopsy is obtained to exclude high metabolic malignancy. Tissue sampling shows histological proof of the pigmented villonodular synovitis (PVNS).

Phosphaturic mesenchymal tumor

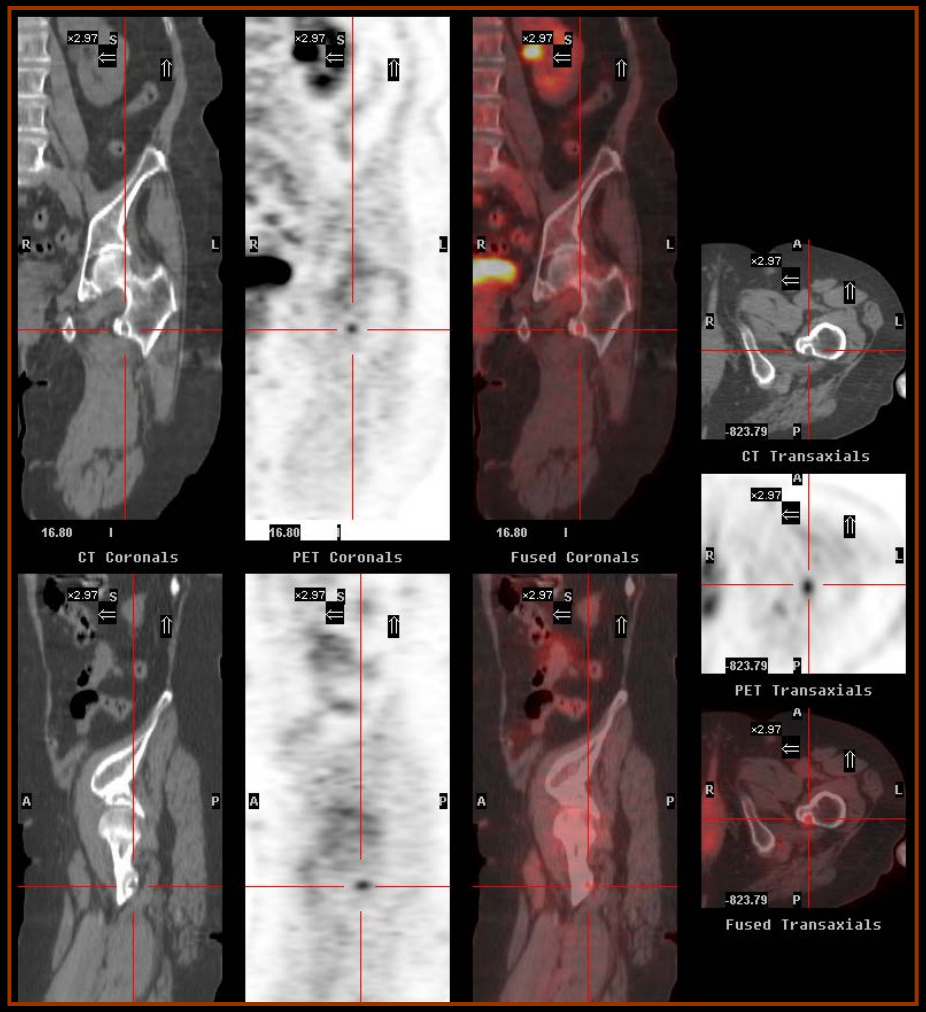

PET/CT reveals the left femoral neck fracture with adjacent small focus of hypermetabolism at the lesser trochanter, which corresponds to a rim-calcified hypodense lesion on CT (left figure, crosshair). At surgical reduction and repair of the femoral neck fracture, this small lesion is resected, with final pathology of fibrohistiocytic tumor compatible with phosphaturic mesenchymal tumor. Corresponding coronal MR image (right figure) of the left femoral neck fracture and overlooked tumor inducing osteomalacia.

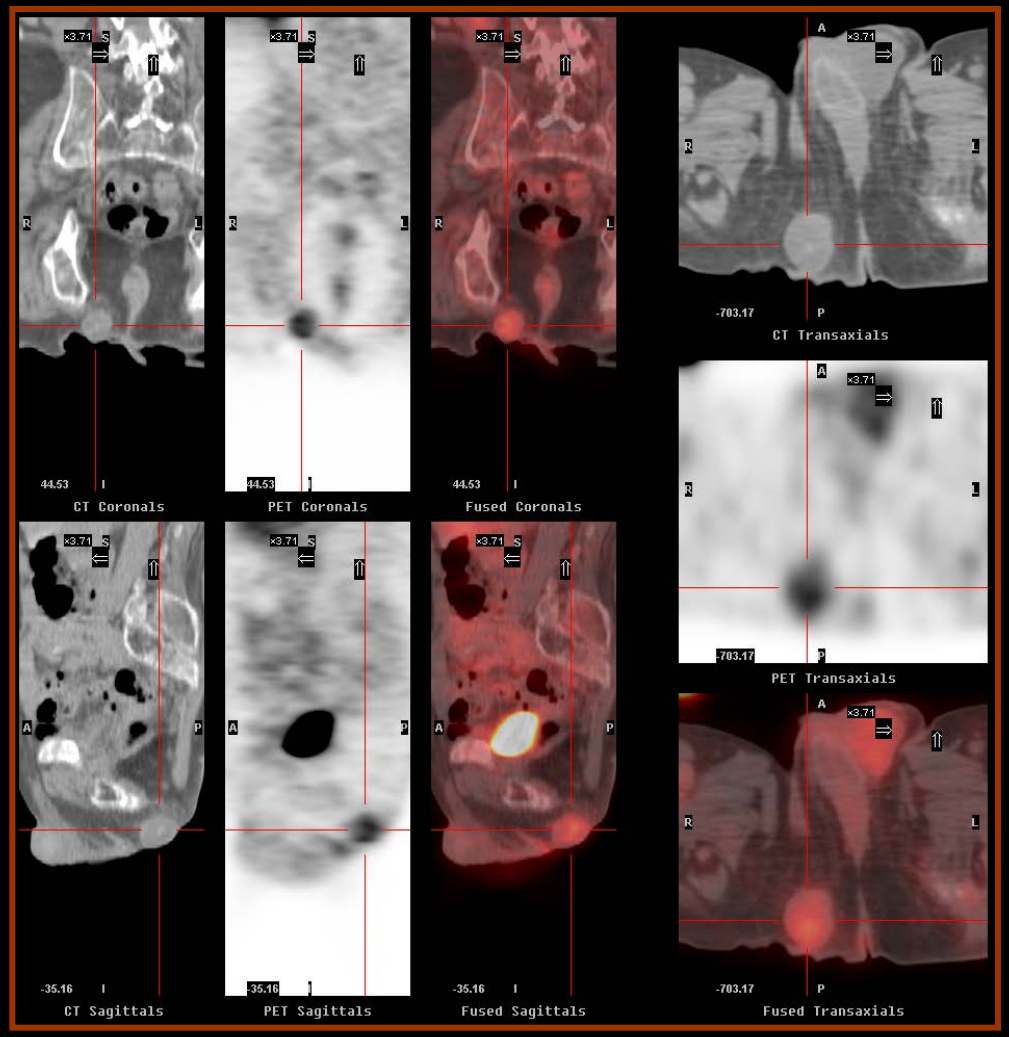

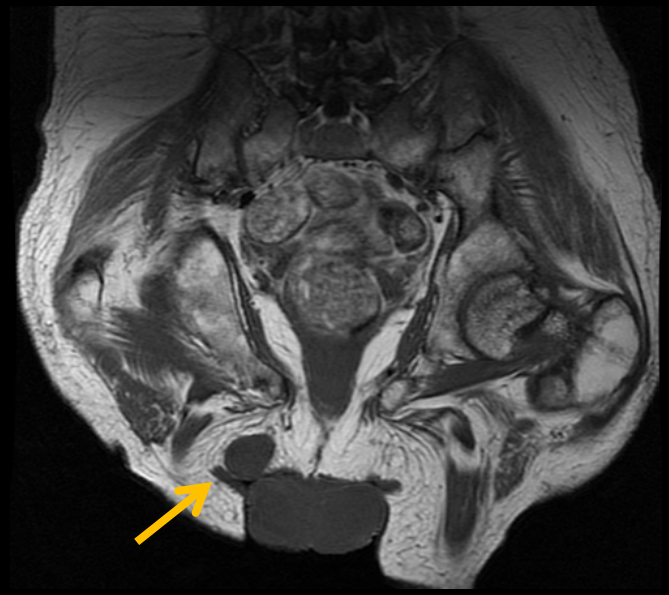

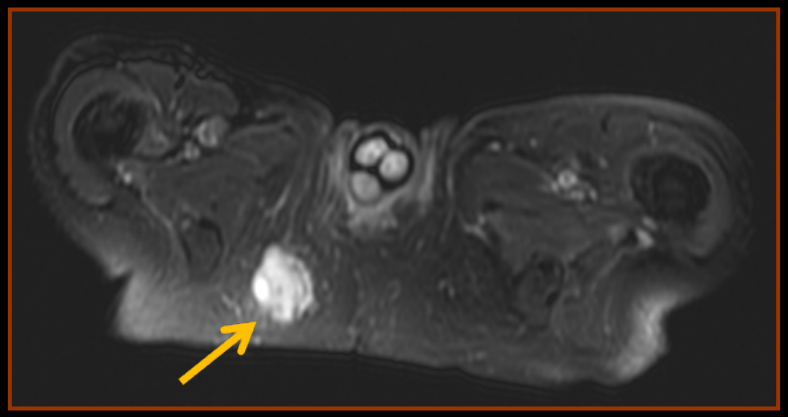

Phosphaturic mesenchymal tumor (continued). PET/CT image shows a focus of abnormal F-18 FDG uptake (SUV: 2.7) at the medial aspect of the right buttock postero-inferior to the right ischium (left figure, crosshair). This finding corresponds to a palpable but asymptomatic soft-tissue nodule neglected by the patient and previously considered benign by clinicians. Coronal T1-weighted image shows a hypo-intense 2.5-cm subcutaneous lesion at the medial aspect of the right buttock (upper right figure) with insufficiency fracture of the left femoral neck. Axial T2-weighted MR image shows the same lesion with increased signal intensity inferior to the right ischial tuberosity (lower right figure). The resected lesion shows histologic evidence of a benign phosphaturic mesenchymal tumor with mixed connective tissue variant. Clinical follow-up of this patient shows progressive normalization of the laboratory values with steady recovery of muscular strength and autonomy.

Hemorrhagic pseudotumor

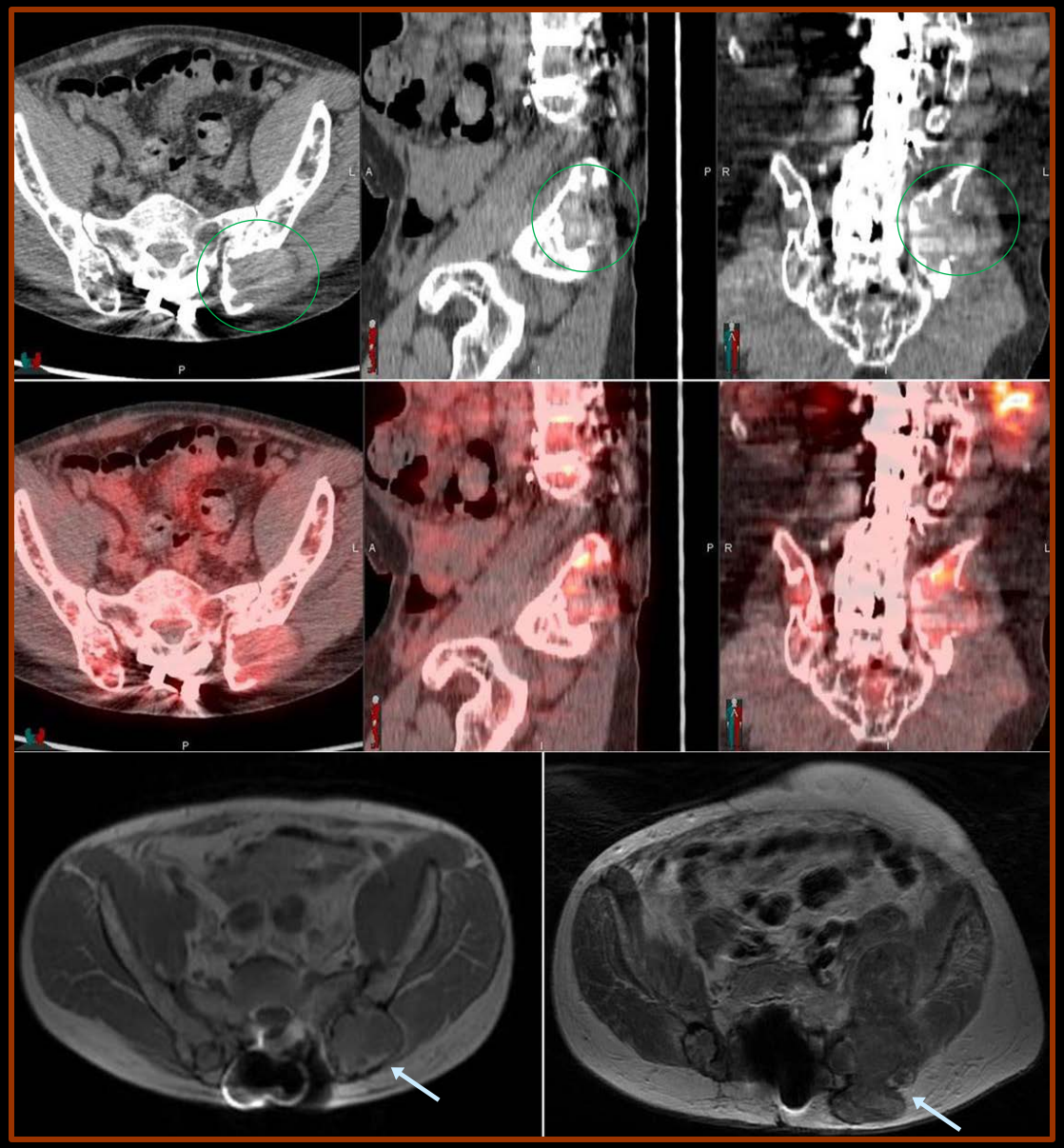

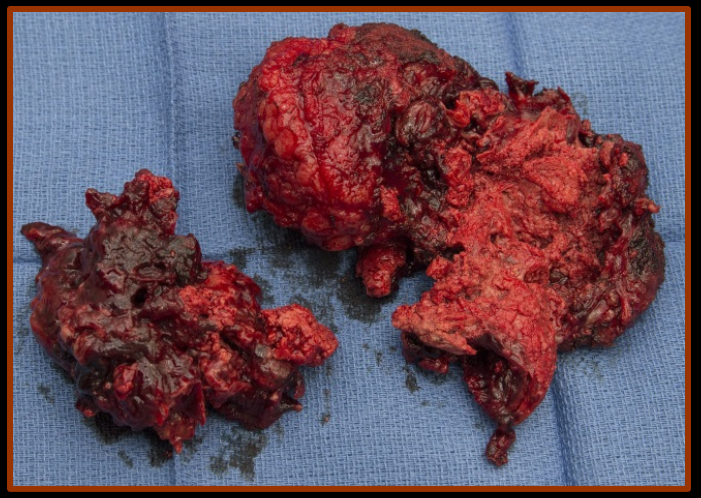

Patient with Noonan's syndrome and enlarging masses of the iliac bones most dominant on the left side depicted by PET/CT (circles)and MR (left images, arrows). PET/CT shows borderline hypermetabolic lesions, which represent hemorrhagic pseudotumor based on the surgical specimen (right). The hemorrhagic pseudotumors are related to the patient's coagulation impairment seen with Noonan's syndrome.

Deltoid chondroid lipoma

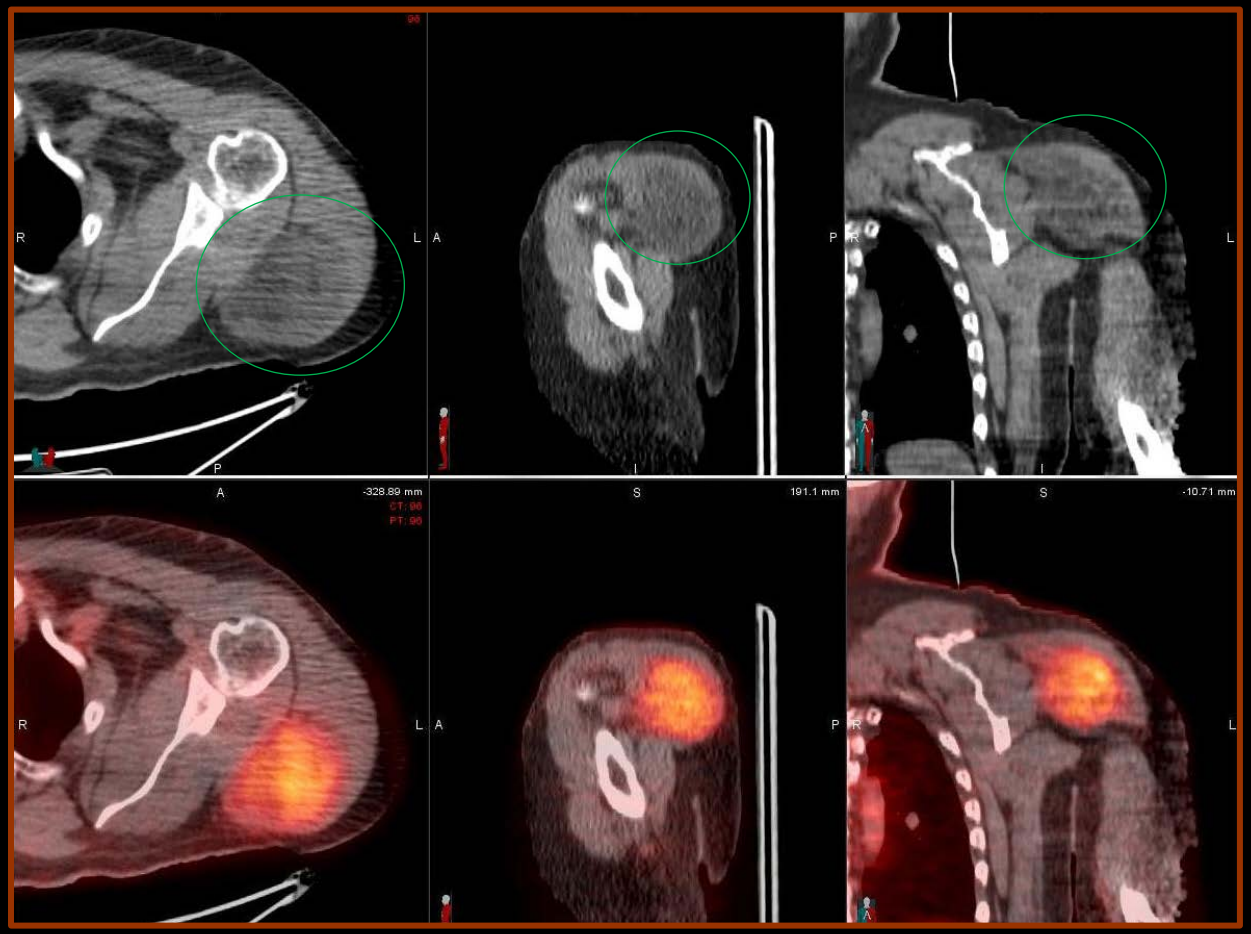

Composite CT (top row) and fused PET/CT (bottom row) images showed a hypermetabolic mass at the posterior aspect of the left deltoid muscle (circles)without any osseous involvement (SUV 3.9-5.5). The tumor had fat tissue attenuation characteristics on transmission CT. The surgically excised specimen photograph shows a well-circumscribed, lobulated, yellowish mass with a thin translucent capsule. Histologically, the tumor was comprised of chondromyxoid-appearing cells and stroma with prominent lipoblasts and adipose tissue, consistent with chondroid lipoma.

Ischiocavernosus myositis

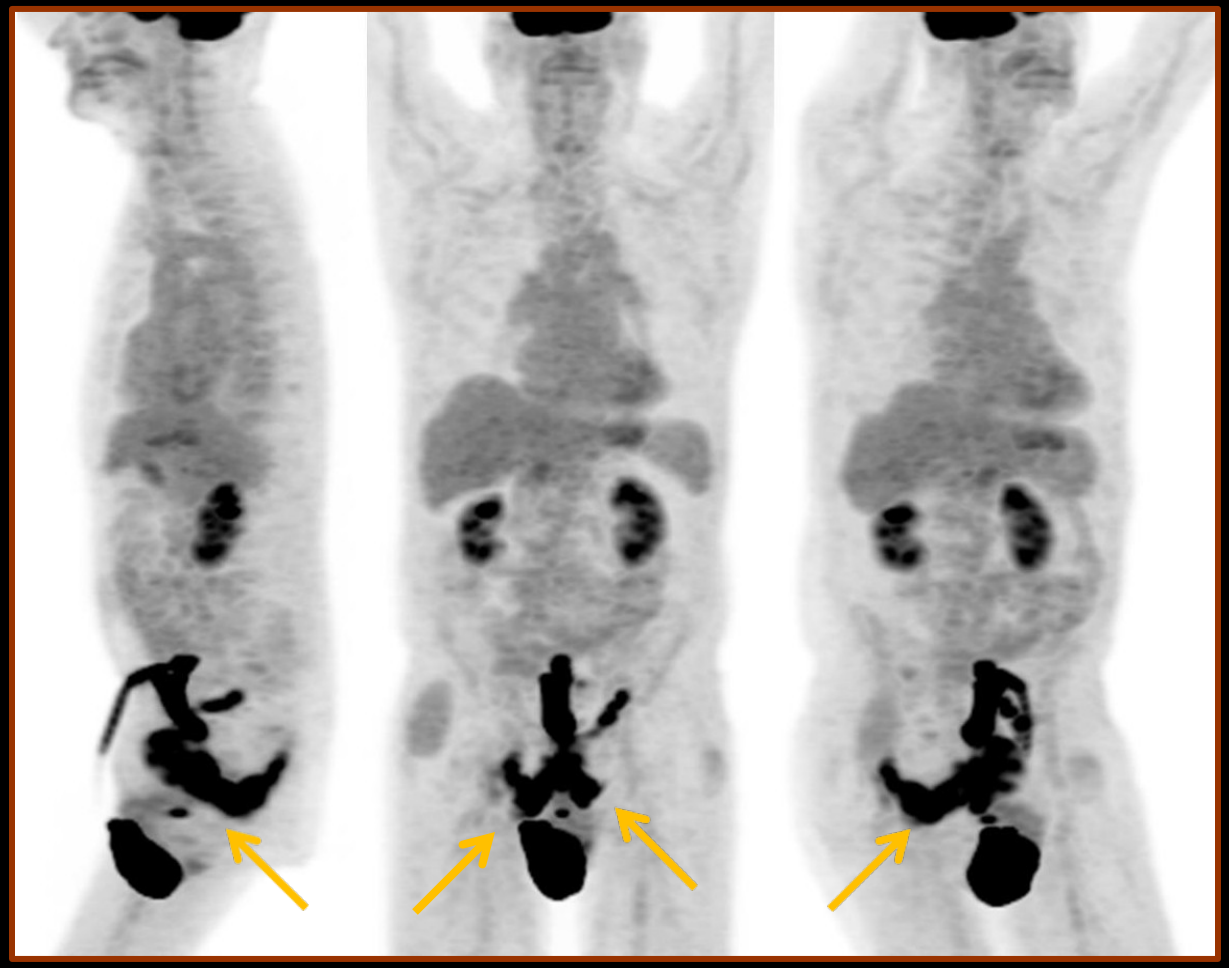

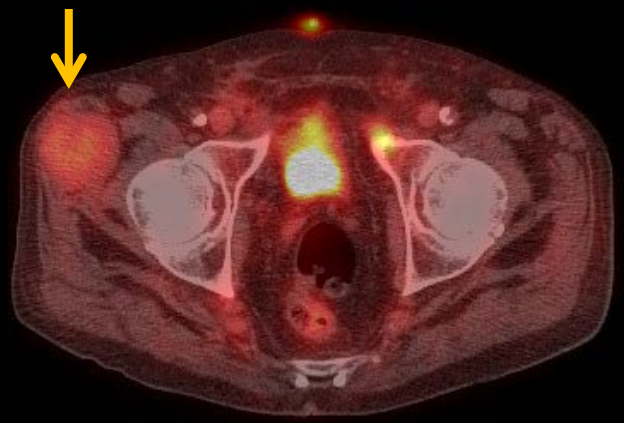

Curvi-linear uptake features of the ischiocavernosus muscles bilaterally abutting both inferior pubic rami (arrows) and to a lesser extend left obturator muscle representing myositis secondary to recurrent inflammation of the pelvis in a patient with suprapubic urinary bladder catheterization and failed artificial urinary sphincter placement Coexisting mildly hypermetabolic fibrous tumor of the right hip (arrow).

Iatrogenic hematoma

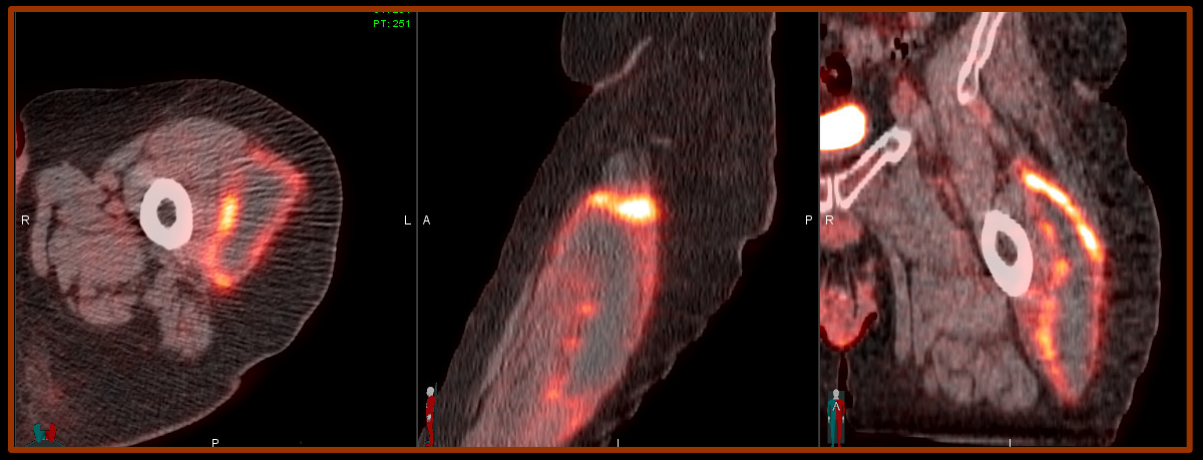

Curvi-linear uptake features and complex appearing soft tissue mass seen on the FDG-PET MIP images (left) and fused PET/CT axial (top left), coronal (top middle), and sagittal (top right) images with a more peripheral pattern of hypermetabolic signal consistent with an iatrogenic hematoma, secondary to anticoagulant therapy, of the lateral left thigh musculature abutting but not involving the left femoral diaphysis.

Osteomyelitis with abscess formation

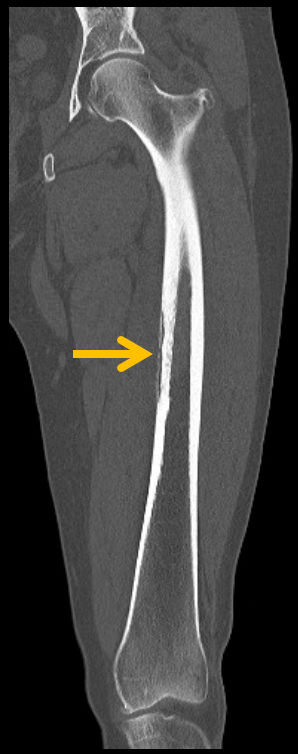

There is an intense focus of uptake seen on the fused PET/CT images (above) and circled in green corresponding with the non-calcified soft tissue mass on coronal CT at the medial aspect of the left femur with direct femoral involvement and evidence of cortical destruction and thickening from osteomyelitis and abscess formation.

Induced polymyalgia rheumatica

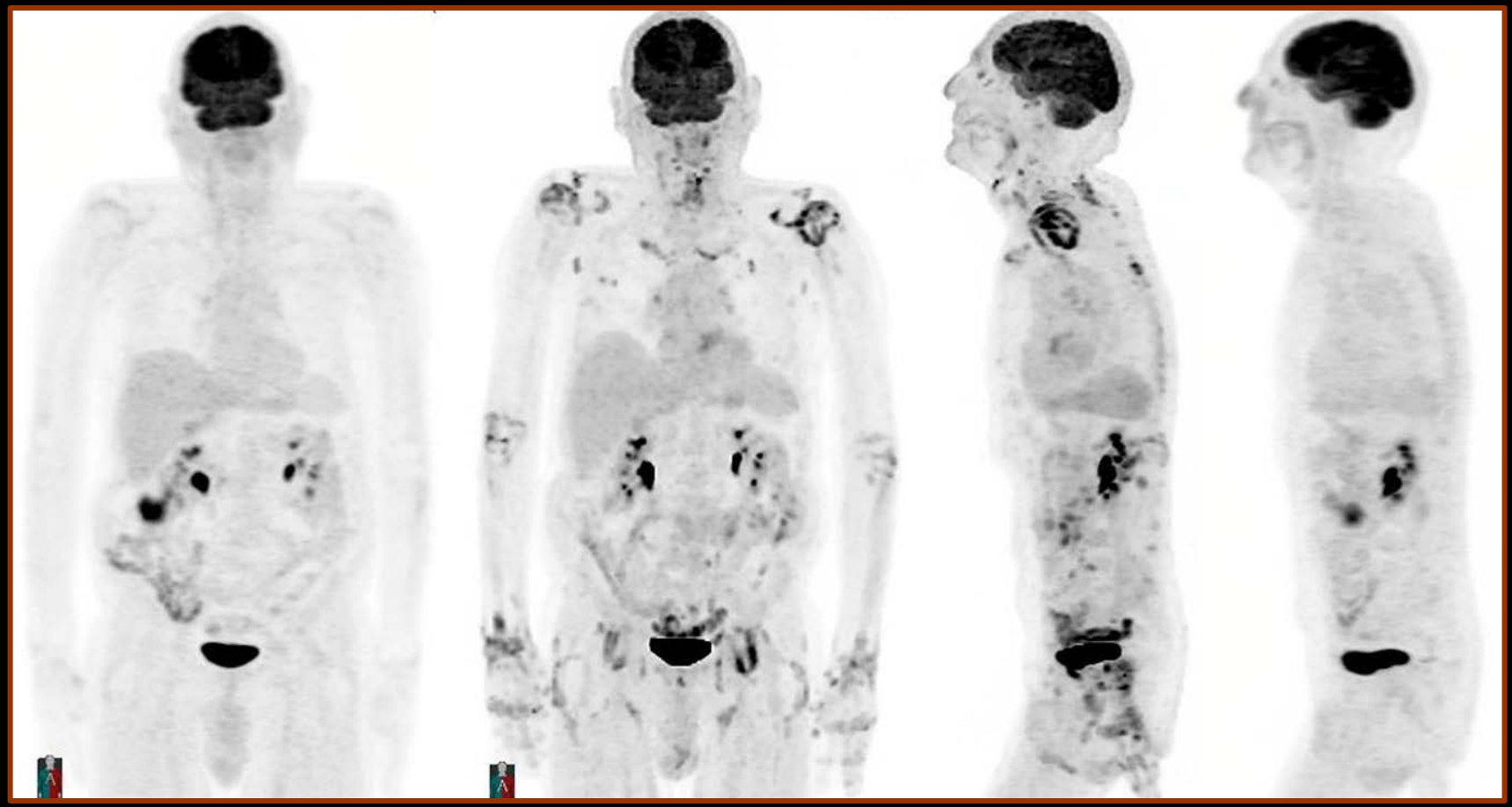

MIP PET images showing curvi-linear uptake features at joint spaces of neck, shoulders, sternoclavicular joints, elbows, wrist, hands, and hips reactive to on-going chemotheraphy (images in the center). These features of induced polymyalgia rheumatica subside after chemotherapy on subsequent PET/CT monitoring.

"TAKE HOME" POINTS

- Familiarity with PET features suggestive of the behavior of the lesions. Benign features tend to be curvi-linear, curvi-tubular, diffuse, symmetrical, geometric, aligned, and anatomic, with absent or low tracer uptake intensity of the lesions. Potentially malignant uptake patterns are random, amorphous, nodular, mass-like, multi-focal, and hypermetabolic (be cautious about the frequent overlap of inflammation/infection and malignancy with regard to the high degree of F-18 FDG uptake of lesions).

- Awareness of physiologic tracer uptake patterns of different organ systems especially musculoskeletal features (e.g. physiologic muscle contraction, brown adipose tissue…).

- Familiarity with the patient's clinical and surgical history to distinguish trauma, iatrogenic, inflammatory, infectious, and post-procedural scintigraphic changes from malignancy.

- Correlation of PET features with corresponding transmission CT anatomic details, and any contemporary imaging such as ultrasound and magnetic resonance imaging, to assess the likelihood of benign and aggressive/malignant behavior of the musculoskeletal processes.

REFERENCES

Choi YY, Kim JY, Yang SO.PET/CT in benign and malignant musculoskeletal tumors and tumor-like conditions. Semin Musculoskelet Radiol. 2014 Apr;18(2):133-48.

Etchebehere EC, Hobbs BP, Milton DR, et al.Assessing the role of (18)F-FDG PET and (18)F-FDG PET/CT in the diagnosis of soft tissue musculoskeletal malignancies: a systematic review and meta-analysis. Eur J Nucl Med Mol Imaging. 2016 May;43(5):860-70.

Sopov V, Bernstine H, Stern D, et al. Spectrum of focal benign musculoskeletal 18F-FDG uptake at PET/CT of the shoulder and pelvis. AJR Am J Roentgenol. 2009 Apr;192(4):1029-35.

Shin DS, Shon OJ, Han DS, et al. The clinical efficacy of (18)F-FDG-PET/CT in benign and malignant musculoskeletal tumors. Ann Nucl Med. 2008 Aug;22(7):603-9.

Nakajo M, Nakajo M, Jinguji M, et al.The value of intratumoral heterogeneity of (18)F-FDG uptake to differentiate between primary benign and malignant musculoskeletal tumours on PET/CT.Br J Radiol. 2015;88(1055):20150552.

Wachsmann JW, Gerbaudo VH.Thorax: normal and benign pathologic patterns in FDG-PET/CT imaging. PET Clin. 2014 Apr;9(2):147-68.

Feldman F, van Heertum R, Manos C. 18FDG PET scanning of benign and malignant musculoskeletal lesions. Skeletal Radiol. 2003 Apr;32(4):201-8.

Strobel K, Stumpe KD. PET/CT in musculoskeletal infection. Semin Musculoskelet Radiol. 2007 Dec;11(4):353-64.

Truong MT, Viswanathan C, Carter BW, et al. PET/CT in the thorax: pitfalls. Radiol Clin North Am. 2014 Jan;52(1):17-25.

Strobel K, Exner UE, Stumpe KD, et al. The additional value of CT images interpretation in the differential diagnosis of benign vs. malignant primary bone lesions with 18F-FDG-PET/CT. Eur J Nucl Med Mol Imaging. 2008 Nov;35(11):2000-8.